Tu N116 03

PS-wave AVAz and Challenges for Joint Inversion

J.E. Gaiser* (CGG Services (US) Inc)

SUMMARY

Changes in fracture direction across interfaces can have an important impact on PS-wave reflection coefficients in azimuthally anisotropic media. Extending conventional joint inversion with P-waves to include amplitude variations with azimuth (AVAz) would use radial and transverse reflection coefficients (RPSV and RPSH, respectively), and present a number of challenges. One of these is that layerstripping (LS) must be done either prior to or during joint inversion with fast PS1- and slow PS2-waves for azimuthal rock properties (e.g., fractures or stress directions). Also, null amplitude directions of RPSH can be shifted in azimuth when fracture direction changes across the interface, and will be different from the actual fracture direction. As a consequence, a full waveform inversion (FWI) approach without registering PS-waves to P-wave time could be more practical than attempting to align them prior to joint AVAz inversion.

Introduction

Shear waves (S-waves) are very sensitive to fracture direction and may be able to help joint P-wave and converted P- to S-wave (PS-wave) amplitude inversion. Tillotson et al. (2012) have shown that S-wave birefringence (splitting) is proportional to crack density in physical model studies. This observation is based on Eshelby's (1957) theory of ellipsoidal inclusions (fluid filled cracks), which has been incorporated in theories for fractured and porous media to model seismic anisotropy (Hudson, 1981; Thomsen, 1995).

Conventional isotropic joint amplitude variation with angle (AVA) inversion (e.g., Dariu et al., 2003, and Barnola and Ibram, 2014) ignores the azimuthally anisotropic effects of splitting into fast (PS_1) and slow (PS_2) converted-waves. However, Jílek (2002) has derived linearized approximations for PS-wave reflection coefficients, R_{PSV} and R_{PSH}, between weakly anisotropic media that could in principle be used for such a joint azimuthal (AVAz) inversion with P-waves.

Inverting for fracture properties may be challenging because layerstripping (LS) must be done prior to or during the inversion to separate the PS_1- and PS_2-waves. Also, null amplitude directions of R_{PSH} can be shifted in azimuth when fracture direction changes across an interface, and could result in errors. LS and AVAz inversion should constrain each other. Therefore, a full waveform inversion (FWI) method that simultaneously incorporates the kinematics of LS and the dynamics of AVAz might be a more practical approach.

In this paper I extend Jílek's (2002) approximations to include higher order coefficients in the angle of incidence, and model R_{PSV} and R_{PSH} amplitudes for orthorhombic media where the fracture direction can change across the interface. For horizontal transversely isotropic (HTI) media, I demonstrate with synthetic data how null directions on the transverse component can be shifted in azimuth with respect to fracture direction, and show similar observations with common receiver gathers (CRGs) from ocean-bottom cable (OBC) data from the Gulf of Mexico.

PS-wave approximations and amplitude modelling

Approximations to reflection coefficients are derived here for R_{PSV} and R_{PSH} as a function of $\sin(\theta)$ and $\sin^3(\theta)$ where θ is vertical angle of incidence and ϕ is azimuth (Jílek 2002). As the subscripts indicate, R_{PSV} is associated with the radial source-receiver direction,

$$\begin{aligned} R_{PSV}(\theta,\phi) = -\Big[& A_{iso} + A_1^{(1)} \sin^2\phi - A_2^{(1)} \sin^2(\phi-\kappa) + A_1^{(2)} \cos^2\phi - A_2^{(2)} \cos^2(\phi-\kappa) \Big] \sin\theta \\ + \Big[& B_{iso} + B_1^{(1)} \sin^2\phi - B_2^{(1)} \sin^2(\phi-\kappa) + B_1^{(2)} \cos^2\phi - B_2^{(2)} \cos^2(\phi-\kappa) \\ & - C_1^{(1)} \sin^4\phi + C_2^{(1)} \sin^4(\phi-\kappa) - C_1^{(2)} \cos^4\phi + C_2^{(2)} \cos^4(\phi-\kappa) \Big] \sin^3\theta, \end{aligned} \tag{1}$$

and R_{PSH} with the transverse direction,

$$\begin{aligned} R_{PSH}(\theta,\phi) = -\Big[& D_1 \sin 2\phi - D_2 \sin 2(\phi-\kappa) \Big] \sin\theta \\ + \Big[& E_1 \sin 2\phi - E_2 \sin 2(\phi-\kappa) - F_1 \sin 4\phi + F_2 \sin 4(\phi-\kappa) \Big] \sin^3\theta, \end{aligned} \tag{2}$$

where angle κ is the change in fracture orientation across the interface. The isotropic coefficients in equation (1) are functions of density, $\Delta\rho/\rho$, S-wave velocity, $\Delta\beta/\beta$, and background V_P/V_S in accordance with Aki and Richards (1980). The other coefficients are anisotropic and also depend on background V_P/V_S where $A_j^{(i)}$ and $B_j^{(i)}$ depend on the Thomsen (1986) parameters δ_{ij} for the i^{th} axis and for the j^{th} layer. The $A_2^{(i)}$ and $B_2^{(i)}$ also depend on S-wave splitting anisotropy, $\gamma^{(S)}$. All terms are defined as in Tsvankin (1997) and resemble Rüger's (2001) in HTI symmetry directions. The $C_j^{(i)}$ depend on the Thomsen (1986) ε_{ij}, and δ_{ij} in the horizontal plane (δ_{31} and δ_{32}). By comparison, R_{PSH} in equation (2) seems relatively simple. There are no isotropic terms, and $D_j^{(i)}$ and $E_j^{(i)}$ have a similar dependence as the $A_j^{(i)}$ and $B_j^{(i)}$, and the $F_j^{(i)}$ have a similar dependence as the $C_j^{(i)}$.

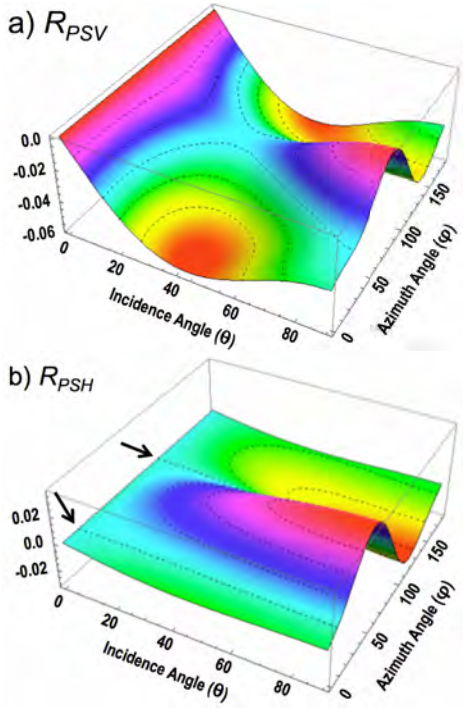

Figure 1 *Reflection coefficients for R_{PSV} (a) and R_{PSH} (b) where S-wave splitting, $\gamma^{(S)}$, is 0.05 but fracture direction changes by –30°. Dashed contours are 0.01 amplitude intervals, and note that the null amplitude contours on R_{PSH} (arrows) are shifted in azimuth and are not aligned with the fracture direction at 90°.*

Figure 1 shows amplitude plots of R_{PSV} and R_{PSH} for orthorhombic incident and reflecting media. The background contrasts for $\Delta\rho/\rho$ and $\Delta\beta/\beta$, are 0.01, and $\gamma^{(S)}$, is 0.05 in both layers, a typical value observed in PS-wave surveys (Gaiser et al., 2001). All the other anisotropy parameters are taken from Jílek's (2002) weak anisotropy example, except that in this case, $\kappa = -30$ degrees (i.e., the fracture direction changes by –30°). The fracture azimuth is 90°.

R_{PSH} show some interesting characteristics that have important consequences for LS. Note that the null amplitude contours (arrows) are shifted in azimuth (approximately +15°) and are not aligned with fracture direction. These null directions are typically identified in the LS process before determining the magnitude of $\gamma^{(S)}$. Although small errors in estimating fracture azimuth are not likely to result in large traveltime errors for $\gamma^{(S)}$, as demonstrated by Gaiser et al. (1997), these errors could be important for joint amplitude inversion.

PS-wave layerstripping examples

PS-wave reflection coefficients are generally not observable in azimuthally anisotropic media unless the kinematic effects of S-wave birefringence are first removed. PS-waves detected on the radial component provide R_{PSV} only when the source-receiver azimuth is aligned with principal directions of the fracture anisotropy. In other azimuths the radial component represents the constructive interference (in general) of the fast and slow PS-waves. Also in these azimuths, the transverse component represents the destructive interference (in general), not R_{PSH}. This situation compromises PS-wave data for conventional joint AVO inversion, and indicates that LS needs to be done before AVAz inversion. However, in media where the fracture direction changes, LS might be even more challenging. In this section I show a synthetic example of LS for HTI layers where the fracture direction changes with depth, and also an OBC example from the Gulf of Mexico.

Synthetic data

Figure 2a shows radial and transverse data labelled with sensor orientations. These data are CRGs where each trace corresponds to common-azimuth stacks in different propagation directions. Radial particle motion is aligned with the propagation direction and transverse particle motion is in the perpendicular direction. There is an isotropic layer (water in the OBC case) over three HTI layers with

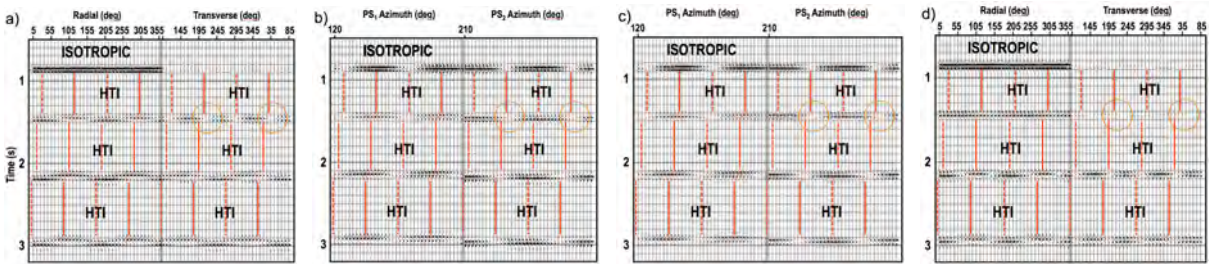

Figure 2 *Layerstripping process of synthetic data for a model with an isotropic layer over three HTI layers where the fracture direction (solid vertical red lines) changes by –15° in each layer. Input radial and transverse common-azimuth stacks (a) are rotated to the fracture direction of the upper HTI layer (b), slow PS_2 reflections are shifted to align with the fast PS_1 reflections (c), and then the data are rotated back to radial and transverse (d) for analysis and processing of the next deeper HTI layer.*

fracture azimuth indicated by solid vertical lines. Dashed lines are directions perpendicular to fractures. The HTI fracture orientation is N120E in the second layer and changes by –15° in each layer. S-wave splitting, $\gamma^{(S)}$, in each layer is 0.0, 0.07, 0.05 and 0.03.

Seismic events in Figure 2a show the characteristic signatures of this fractured medium. The earliest event shows a strong response on the radial component between 0.8 and 0.9 s, but note that there is a small amount of energy on the transverse component. This cannot originate from out-of-plane displacement of the P-wave arrival in the isotropic layer above the interface. These small events are related to continuity of displacement at the interface when P-waves convert to downgoing transmitted S-waves in the HTI medium. The reflections below this first event show the characteristic signature of interference between PS_1 and PS_2 split S-waves. The fast and slow S-waves continuously separate in time on the radial component with increasing traveltime.

Conventional LS is illustrated in Figure 2 for the reflection at about 1.5 s. After rotation to principal directions (Figure 2b), null amplitude responses normally coincide with the fracture direction. However, we see that this is not precisely true (circles). An estimate of reflection coefficients, R_{PSV} and R_{PSH} (Figure 2d) are obtained by removing the slow PS_2-wave delay (–28 ms) and aligning it with the fast PS_1-wave (Figure 2c), and then rotating back to radial and transverse. R_{PSV} amplitude varies elliptically in azimuth and is low amplitude in the fracture direction, and R_{PSH} has a $\sin(2\phi)$ behaviour with polarity reversals every 90° in azimuth. However, note that the AVAz signature of R_{PSH} does not entirely agree with the LS parameters that would have been estimated and used to identify fracture direction. The null amplitude direction of R_{PSH} that would have been picked is consistently shifted in azimuth (circles in Figure 2). This situation highlights the importance that the kinematics of LS (splitting and perhaps NMO) and amplitude inversion should describe a consistent model. They need to be inverted simultaneously as in a FWI method.

OBC Gulf of Mexico data

Similar birefringence signatures can be observed from the Teal South area in the Gulf of Mexico. Figure 3 shows common-azimuth stacks, before (3a) and after (3b) LS (three layers). Note that the direct P-wave arrival in Figure 3a has a small amount of high frequency transverse energy, exhibiting a $\sin(2\phi)$ behaviour. Although this suggests that the seabed is azimuthally anisotropic, the direct arrival and earliest reflections on the radial component are essentially flat. By 1.5 s however, the fast and slow reflections are clear on the radial component, at about N115E and N205E, respectively, and exhibit a sinusoid-like interference with azimuth. Also, the null amplitude directions become well defined on the transverse component. After 2.0 s, PS_1 and PS_2 are completely separated in time.

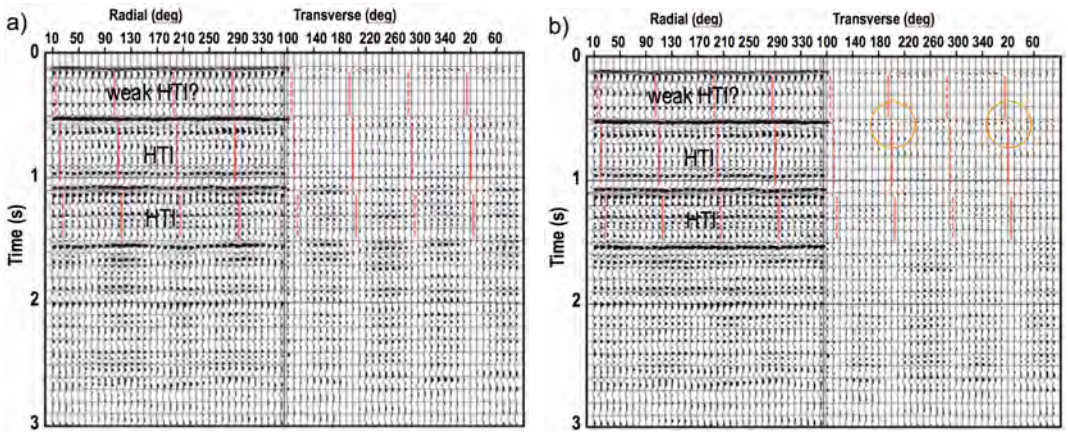

Figure 3 *Common-azimuth stacks from Teal South in the Gulf of Mexico shows three layers determined by layerstripping: an isotropic (or weak HTI) layer over two HTI layers where the inferred fracture directions are indicated by solid vertical red lines that appear to change in azimuth. The input radial and transverse data (a) are analyzed for null amplitude directions on the transverse (fracture direction), and traveltime differences between PS_1 and PS_2 on the radial (fracture intensity, $\gamma^{(S)}$). After layerstripping (b), radial and transverse components represent the reflection coefficients, R_{PSV} and R_{PSH}, respectively.*

Layerstripping to 1.5 s (three layers with $\gamma^{(S)}$: ~0.0, 0.01 and 0.03) aligns reflections on the radial component with more consistent azimuthal amplitude response, and produces the characteristic residual amplitudes on the transverse component. These responses represent estimates of R_{PSV} and R_{PSH}. Note that the event at 0.5 s (circle) now shows a clear sin(2ϕ) behaviour on transverse compared with Figure 3a; however, the null amplitude direction of this event does not appear to be aligned with the kinematic estimate of the principal directions. The actual fracture directions are of course unknown. For events from around 1.0 to 1.5 s there appears to be closer agreement of the estimated principal directions and the null amplitude directions. Further LS is required after 1.5 s. Nevertheless, a joint inversion solution will need to have consistent traveltimes and amplitude models.

Conclusions

Layerstripping (LS) must be done prior to or during amplitude inversion of PS_1- and PS_2-waves for azimuthal rock properties (e.g., fractures or stress directions). However, null amplitude directions of R_{PSH} will be shifted in azimuth when fracture direction changes across the interface, and will be different from the actual fracture directions, resulting in LS errors. LS and AVAz inversion should be done together such that traveltime and amplitude models are consistent with each other. A more practical approach may be FWI that simultaneously incorporates the kinematics of LS with the dynamics of AVAz.

Acknowledgements

I thank Petr Jílek and Ilya Tsvankin for very interesting and helpful discussions, and CGG for permission to publish this material.

References

Aki, K., and Richards, P.G. 1980. Quantitative Seismology: theory and methods. **1**, *W.N. Freeman and Co.*, San Fransisco.

Barnola, A.S., M. Ibram. 2014. 3D simultaneous joint PP-PS prestack seismic inversion at Schiehallion field, United Kingdom continental shelf. *Geophys. Prosp.* **62**, 278–292.

Dariu, H., P.Y. Granger, J.P. Fjellanger and P. Risti. 2003. Multicomponent AVO inversion using simulated annealing. *65th Conf. and Exhib. EAGE*, Ext. Abs. **D16**.

Eshelby, J.D. 1957. The determination of the elastic field of an ellipsoidal inclusion, and related problems. *Proceedings of the Royal Society* **A241**, 376–396.

Hudson, J.A. 1981. Wave speeds and attenuation of elastic waves in material containing cracks: Geophys. J.R. aster. Soc. **64**, 133–150.

Gaiser, J.E., P.J. Fowler and A.R. Jackson. 1997. Challenges for 3-D converted-wave processing. *67th Ann. Int. Mtg. SEG*, Exp. Abs. **SP5.2**, 1199–1202.

Gaiser, J., R. Van Dok and J. Markert. 2001. Processing and analysis of PS-wave data from a 3-D/3-C land survey for fracture characterization. *63rd Conf. & Tech. Exhib. EAGE*, Ext. Abs., **P117**.

Jílek, P. 2002. Modeling and inversion of converted PS-wave reflection coefficients in anisotropic media: a tool for quantitative AVO analysis. *Colorado School of mines, Doctoral Thesis* **CWP 400**.

Rüger, A., 2001, Reflection coefficients and azimuthal AVO analysis in anisotropic media: Geophysical monograph series, **10**, Society of Exploration Geophysicists.

Thomsen, L. 1986. Weak elastic anisotropy. *Geophysics* **51**, 1954–1966.

Thomsen, L. 1995. Elastic anisotropy due to aligned cracks in porous rock. *Geophys. Prosp.* **43**, 805–829.

Tillotson, P., J. Sothcott, A.I. Best, M. Chapman and X.Y. Li. 2012. Experimental verification of the fracture density and shear-wave splitting relationship using synthetic silica cemented sandstones with a controlled fracture geometry. *Geophys. Prosp.* **60**, 516–525.

Tsvankin, I. 1997. Anisotropic parameters and P-wave velocity for orthorhombic media. *Geophysics* **62**, 1292–1309.